



UNIVERSITY OF LEEDS

This is a repository copy of *Rapid Screening of Calcium Carbonate Precipitation in the Presence of Amino Acids: Kinetics, Structure, and Composition*.

White Rose Research Online URL for this paper:

<https://eprints.whiterose.ac.uk/103269/>

Version: Accepted Version

Article:

Green, DC orcid.org/0000-0002-0578-2369, Ihli, J orcid.org/0000-0002-9541-5748, Kim, Y-Y orcid.org/0000-0002-8503-4554 et al. (4 more authors) (2016) Rapid Screening of Calcium Carbonate Precipitation in the Presence of Amino Acids: Kinetics, Structure, and Composition. *Crystal Growth and Design*, 16 (9). pp. 5174-5183. ISSN 1528-7483

<https://doi.org/10.1021/acs.cgd.6b00741>

© 2016 American Chemical Society. This document is the Accepted Manuscript version of a Published Work that appeared in final form in *Crystal Growth and Design*, copyright © American Chemical Society after peer review and technical editing by the publisher. To access the final edited and published work see <http://dx.doi.org/10.1021/acs.cgd.6b00741>.

Reuse

Items deposited in White Rose Research Online are protected by copyright, with all rights reserved unless indicated otherwise. They may be downloaded and/or printed for private study, or other acts as permitted by national copyright laws. The publisher or other rights holders may allow further reproduction and re-use of the full text version. This is indicated by the licence information on the White Rose Research Online record for the item.

Takedown

If you consider content in White Rose Research Online to be in breach of UK law, please notify us by emailing eprints@whiterose.ac.uk including the URL of the record and the reason for the withdrawal request.



eprints@whiterose.ac.uk
<https://eprints.whiterose.ac.uk/>

Rapid-Screening of Calcium Carbonate Precipitation in the Presence of Amino Acids: Kinetics, Structure and Composition

David C. Green^a, Johannes Ihli^{a†}, Yi-Yeoun Kim^a, Samantha Y. Chong^b, Phillip A. Lee^a, Christopher J. Empson^a and Fiona C. Meldrum^{a*}

^aSchool of Chemistry, University of Leeds, Leeds, LS2 9JT, UK; ^bDepartment of Chemistry, University of Liverpool, Liverpool, L69 7ZD, UK.

Soluble additives are widely used to control crystallization, leading to definition of properties including size, morphology, polymorph and composition. However, due to the number of potential variables in these experiments, it is typically extremely difficult to identify reaction conditions – as defined by solution compositions, temperatures and combinations of additives – that give the desired product. This article introduces a high-throughput methodology which addresses this challenge and enables the streamlined preparation and characterization of crystalline materials. Using calcium carbonate precipitated in the presence of selected amino acids as a model system, we use well plates as micro-volume crystallizers, and an accurate liquid-handling pipetting workstation for sample preparation. Following changes in the solution turbidity using a plate reader delivers information about the reaction kinetics, while semi-automated scanning electron microscopy, powder XRD and Raman microscopy provide structural information about the library of crystalline products. Of particular interest for the CaCO₃ system is the development of fluorescence-based protocols which rapidly evaluate the amounts of the additives occluded within the crystals. Together, these methods provide a strategy for efficiently screening a broad reaction space, where this can both accelerate the ability to generate crystalline materials with target properties, and develop our understanding of additive-directed crystallization.

INTRODUCTION

The development of methods to control crystallization processes is of great importance to a vast number of natural and technological processes. These range from the production of pharmaceuticals, nanomaterials, ceramics and biomaterials, to environmental processes including weathering and carbon-capture, to the prevention of unwanted crystallization in the form of scale or pathological mineralization such as kidney stones. One of the most important strategies employed to achieve this goal is the use of soluble additives; where these provide an experimentally straightforward means of defining features including polymorph, morphology, size and size distribution.¹⁻³ There is no better demonstration of the power of this approach than biomineralization, where the manipulation of inorganic materials by organic molecules is central to the ability of organisms to form structures such as bones, teeth and seashells.⁴⁻⁶ This strategy enables nature to gain enviable control over features such as polymorph and morphology, and occlusion of macromolecules within the crystal lattice can lead to crystals with superior mechanical properties⁷ and modified textures.^{8,9}

Inspired by biomineralization processes, a wide range of organic additives, including biomacromolecules, block copolymers and small organic species, have been explored to control the precipitation of inorganic crystals.¹ These additives can also become incorporated within the crystal lattice,¹⁰⁻¹⁴ where this is recognized not only for the introduction of impurities into crystals,¹⁵⁻¹⁷ but has also been used to enhance the mechanical properties of calcite,^{13,18} to change the bandgap of ZnO,¹⁹ and to endow the host crystal with new properties, such as color, fluorescence or magnetism.²⁰⁻²³ Understanding the mechanisms of additive occlusion, and the structure/ property relationships of the product doped crystals, however, relies upon the ability to quantify the amount of additives occluded under different growth conditions. This has been well-studied for atomic occlusions (such as inorganic ions) which are readily quantified using techniques including atomic absorption,²⁴ EXAFS,^{25, 26} or EPR.^{27, 28} Particulate additives can also be easily visualized using electron microscopy or atomic force microscopy²⁹ and quantified with thermal analysis.^{18, 21, 22, 30, 31} The quantification of occluded small organic molecules remains more challenging, however,^{13, 14, 19} unless they have a key signature such as fluorescence.

The ultimate goal of additive-directed crystallization is undoubtedly to be able to pre-select additives and experimental conditions to give a desired product. Due to limitations in our understanding of crystal nucleation and growth processes, however, this remains impossible in most cases and identification of reaction conditions and additives that give the desired product is typically achieved by performing a huge number of experiments comprising different solution conditions, concentrations and even combinations of additives.³² In the work described here, we address this issue by developing a high-throughput method

to study the influence of organic additives on the precipitation of inorganic crystals. Such combinatorial approaches enable the rapid evaluation of a wide reaction space and are well-suited to crystallization studies. They have been used in both the pharmaceutical industry,³³ and for protein crystallization trials,^{34, 35} and are also attracting increasing interest from the perspective of materials discovery,^{36, 37} where they have been shown to be well-suited to the identification and optimization of inorganic thin films for applications such as catalysis.^{38, 39} Using calcium carbonate precipitated in the presence of amino acids (Asp, Glu, Asn and Val) as a model system, we have developed high throughput methods which enable us to precipitate crystals under a wide range of experimental conditions, to analyse the kinetics of the precipitation process using turbidimetry, and to determine the properties of the product crystals using electron microscopy, Raman spectroscopy and powder XRD. In particular, we have established protocols based on fluorimetry to rapidly evaluate the amounts of the additives occluded within the crystals, where this facilitates a detailed investigation of the dependency of occlusion on the solution conditions. These methods offer high reproducibility, require small quantities of reagents and are labor efficient; they are ideally suited to this type of study. By enabling the efficient evaluation of a wide parameter space these methods open the door to the characterization of a wide range of additive/ crystal systems, where researchers can adapt the methodology and “mix and match” characterization techniques appropriate to their crystal systems and the specific information they wish to obtain. Such approaches can help develop our understanding of additive-directed crystallization and the structure/ property relationships of the crystals.

RESULTS

Overview and Experimental Design: Calcite growth in the presence of the amino acids aspartic acid (Asp), glutamic acid (Glu), asparagine (Asn) and valine (Val) was selected for study as although it is recognized that calcite can effectively occlude some amino acids,^{13, 14} the influence of the experimental conditions on incorporation is poorly documented. This system is also amenable to study by a wide range of characterization techniques that can be employed using a high-throughput approach. Figure 1 and Figure S1 provide schematic diagrams of the sample generation and characterization methods employed in this study. A range of strategies for high-throughput sample preparation were developed to enable characterization of the reaction kinetics of CaCO₃ precipitation in the presence of the different amino acids, and the product materials. Properties determined include the mass precipitated, the polymorphs produced (using powder XRD (pXRD) and Raman microscopy), the size and morphologies of the particles as determined by scanning electron microscopy (SEM) and the amounts of amino acids incorporated, as

achieved using fluorescence spectroscopy. The crystallization reactions were carried out within 96-well plates, and each well was loaded with accurate volumes of aqueous solutions using a liquid handling pipetting workstation (Hamilton Microlab STAR). This enabled up to 96 experiments to be performed simultaneously, using the same stock solutions and laboratory conditions (e.g. temperature).

An extensive description of the experimental methods and sample preparation protocols for each of the characterization techniques employed is provided in the Supporting Information. Briefly, experiments were designed to determine the 3-way relationship between the $[\text{Ca}^{2+}]$, the $[\text{amino acid}]/[\text{Ca}^{2+}]$ ratio and the property under investigation. Values of $[\text{Ca}^{2+}] = [\text{CO}_3^{2-}] = 3.5, 5, 7.5$ and 10 mM and $[\text{amino acid}]/[\text{Ca}^{2+}] = 0, 0.3, 0.6, 0.9$ and 1.5 were employed, giving 20 experiments per amino acid, with the exception of the kinetic studies, where only concentrations of $[\text{Ca}^{2+}] = [\text{CO}_3^{2-}] = 10$ mM were examined (providing 5 experiments per amino acid). In all cases, well plates were charged with DI water, followed by aqueous solutions of CaCl_2 and amino acid, and finally an aqueous solution of Na_2CO_3 in order to initiate the reaction. Crystallization was then allowed to proceed over 2 days prior to protocol-specific post reaction treatment and characterization, with the exception of the kinetic studies, where characterization and reaction initiation were performed simultaneously.

Experiments were planned and designed using well plate 'maps' which were tailored to the requirements of each characterization technique. Examples of the experimental maps used for the kinetics and SEM/Raman/pXRD analysis are shown in Figure 2. For the kinetic studies, wells were allocated for $[\text{amino acid}]/[\text{Ca}^{2+}] = 0$ in column 1, while columns 2 and 3 were divided into 4 equal sections of 4 wells to accommodate all of the $[\text{amino acid}]/[\text{Ca}^{2+}]$ values under investigation (Figure 2a). These experimental conditions were repeated across the entire well plate to provide five repeats of each experiment. For samples for analysis by SEM, Raman and pXRD, Rows A-D of column 1 corresponded to $[\text{amino acid}]/[\text{Ca}^{2+}] = 0$ for $[\text{Ca}^{2+}] = [\text{CO}_3^{2-}] = 3.5, 5, 7.5$ and 10 mM respectively. 4×4 grids for all $[\text{Ca}^{2+}] = [\text{CO}_3^{2-}] = 3.5, 5, 7.5$ and 10 mM and $[\text{amino acid}]/[\text{Ca}^{2+}] = 0.3, 0.6, 0.9$ and 1.5 experiments were used for the 4 amino acids on a single well plate (Figure 2b). For the studies of amino acid incorporation, a well plate layout was designed to enable the evaluation of 2 different amino acids in duplicate across the selected parameter space as 4×4 grids (e.g. rows A-D and columns 2-5 inclusive) for $[\text{Ca}^{2+}] = [\text{CO}_3^{2-}] = 3.5, 5, 7.5$ and 10 mM and $[\text{amino acid}]/[\text{Ca}^{2+}] = 0.3, 0.6, 0.9$ and 1.5 . Wells containing amino acids only were also present for the purposes of calibration (columns 1, 6, 7 and 12) (Figure S2). Analysis of all 4 amino acids therefore required the used of 2 separate plates. Control experiments for both $[\text{Ca}^{2+}]$ determination and incorporation studies were performed on a separate plate. An identical well plate layout to that used for incorporation studies was used for calcium concentration determination.

Kinetics: Kinetics studies were performed using turbidimetry to investigate the influence of the amino acids on the precipitation of CaCO_3 , where changes in light transmittance due to particulate light scattering are recorded as a monochromatic beam passes through a precipitation solution. This generates an overview of the early reaction profile, and can provide information on the precipitation of amorphous calcium carbonate (ACC) and its subsequent transformation into crystalline polymorphs.⁴⁰ The benefit of this approach was demonstrated for reaction solutions comprising $[\text{CO}_3^{2-}] = 10 \text{ mM}$ and $[\text{amino acid}]/[\text{Ca}^{2+}] = 0, 0.3, 0.6, 0.9$ and 1.5 for each amino acid (Figure 3). All kinetic studies were conducted in Greiner μClear Black 96-well plates, which have transparent bases, and each well was analyzed simultaneously in a plate reader (PerkinElmer EnVision 2103). The well plates were charged with selected volumes of aqueous CaCl_2 and amino acid solutions using the liquid handling pipetting workstation, while the aqueous Na_2CO_3 solution was subsequently added within the plate reader using the dispenser accessory. This allowed data acquisition to be initiated at the outset of the reaction, thus minimizing the time delay between the first reading and reaction initiation. It is noted that the configuration of these experiment differs from that of traditional UV-Vis spectrometers in that the light-path is vertical through the sample, rather than horizontal (Figure S3). This influences the shape of the reaction profile as both the initial ACC sedimentation and subsequent ACC dissolution/ crystal growth steps can be observed.

The kinetic study demonstrated that the amino acids influenced the stability of ACC to varying degrees. Representative normalized transmittance vs. time plots are shown in Figure 3, where these exhibit an initial drop in transmittance due to the formation of ACC, and then a subsequent recovery as the ACC transforms into much larger crystalline particles. These plots demonstrate that Asp significantly stabilizes the ACC, as indicated by the fact that the maximum absorbance and dissolution/crystal growth phase occur at later times (Figure 3a). This effect was also observed, but to a lesser extent, with Glu and Asn, while Val had little effect on CaCO_3 precipitation. This trend was also shown by plotting a graph of the time corresponding to maximum absorbance against the $[\text{amino acid}]/[\text{Ca}^{2+}]$ ratio for the different amino acids (Figure 3b); each point plotted represents the average of 5 experiments. This pattern of behavior is consistent with previous studies,⁴⁰ where this can be attributed to the charged amino acids inhibiting growth of the crystalline phases, such that the lifetime of the ACC is extended,⁴¹ and reducing the solution supersaturation through chelation effects.

Powder XRD (pXRD): The polymorphs of the crystals precipitated were identified using pXRD, where CaCO_3 can precipitate in three anhydrous polymorphs at room temperature: calcite, aragonite and vaterite. The crystallization experiments were performed in Greiner μClear Black well plates using the maximum solution volume ($300 \mu\text{L}$) in each well and $[\text{Ca}^{2+}] = 7.5 \text{ mM}$ and 10 mM in order to maximize the

yield of crystals (and thus the XRD signal intensity). pXRD was then performed *in situ* within the wells using a PANalytical X'Pert Pro diffractometer with a well plate sample holder, where this enabled automated data acquisition. Diffraction patterns were obtained in transmission mode through the well plate bottom in the range $2\theta = 27-37^\circ$ (scan time of 30 min per well), where this exhibits peaks characteristic of calcite (intense, sharp peaks at $2\theta = 29^\circ$ and 36° ; (104) and (110) respectively), aragonite (peaks at $27-28^\circ$, $32-33^\circ$ and $36-37^\circ$; (021), (012) and (200) respectively) and vaterite (broad peak at $2\theta = 32-33^\circ$; (114)).

This high throughput method was shown to be successful in rapidly determining the crystal polymorphs precipitated in each of the reaction solutions. The data demonstrated that calcite was the sole crystalline phase in all experiments, as shown by the absence of any peaks corresponding to aragonite or vaterite. A representative pattern is given in Figure 4, and all patterns can be found online in the supporting dataset.⁴² This result demonstrates that quantification of amino acid occlusion within the crystal particles corresponds to incorporation within calcite crystals rather than vaterite or aragonite. As the latter two polymorphs are typically polycrystalline when precipitated at room temperature, occlusion data can correspond to amino acids entrapped both within and between the crystallites.

Scanning Electron Microscopy (SEM): The morphologies of the product calcite crystals were determined using SEM. Soluble additives can strongly influence calcite morphologies through preferential association with the acute or obtuse step edges, or pinning of step movement.⁴³⁻⁴⁵ The effect of Asp on calcite growth has been particularly well-studied, where preferential binding to the acute step edges ultimately gives rise to elongated particles with highly roughened sides, that are capped at each apex with three, smooth {104} faces.^{13, 46} At higher supersaturations and additive concentrations calcite can also form polycrystalline particles. Automated SEM analyses were carried out to identify whether the calcite crystals were single crystal or polycrystalline in structure, where this result is particularly important for the interpretation of the additive occlusion data. It is also emphasized that the current set of experiments were designed to give calcite single crystals as products, such that we could examine amino acid occlusion within single crystals. The same protocols could be readily used to examine the morphological effects of organic additives over a wide range of solution conditions.

SEM was performed on crystals precipitated on well plate sealing mats. All aqueous solutions and DI water were added to Greiner μ Clear Black well plates using the liquid handling pipetting workstation. Immediately after initiation of the reaction, the well plate was sealed with a sealing mat (Corning) such that indexed studs on sealing mats corresponded to the same wells on the well plate (i.e. A1 to A1, E6 to E6 etc.) and was then inverted such that the sealing mat was on the bottom. After 2 days crystallization,

the sealing mats were peeled from the well plate and rinsed with ethanol to terminate crystallization and facilitate drying; advantageously, the CaCO_3 crystals bound strongly to the sealing mats. The sealing mats were then cut with scissors into 6x8 sections and mounted onto aluminum sample holders using copper tape, coated with 2 nm Ir and examined with an FEI Nanoscope Nova 450. Navigation and image acquisition was undertaken automatically with MAPS software, or manually using a NavCam accessory where required.

Calcite was identified by its characteristic rhombohedral morphology, which was modified in the presence of amino acids. The most marked changes in morphology occurred in the presence of Asp (Figure 5), which induced a roughening of edges and surfaces. This was most pronounced in $[\text{Ca}^{2+}] = [\text{CO}_3^{2-}] = 10$ mM samples, and across all $[\text{Ca}^{2+}]$ at $[\text{Asp}]/[\text{Ca}^{2+}] = 1.5$. Although most of the crystals were calcite single crystals, some polycrystalline particles were also present in higher $[\text{Ca}^{2+}]$ and $[\text{Asp}]/[\text{Ca}^{2+}]$ samples (Figure S4). This effect was less pronounced for Glu and no significant change was observed with Asn and Val (Figure S5). This trend, where the amino acids with carboxylic acid functionalized side groups are effective calcite growth modifiers, is attributed to strong binding to the calcite surfaces, and can be compared with the effect of Val, which with a hydrophobic side group does not modify the morphology at all. Shape modification therefore primarily derives from the functionality of the side chain as opposed to the α -amino acid moiety. Circularity measurements were also explored using image analysis and were consistent with Asp and Glu causing the greatest change in shape – likely due to polycrystal formation. However, high variability in values where no significant shape change was observed suggested that calcite was not an ideal material for this type of analysis (Figure S6).

Raman Microscopy: Raman spectroscopy provides an effective means of investigating the degree of disorder generated in crystals due to the occlusion of additives.⁴⁷ The positions and widths of the molecular vibrations are directly related to the atomic configurations and the environments of the carbonate groups, and thus provide information about the disorder in the structure. This effect was initially investigated by precipitating calcite crystals in the presence of Asp, recording their Raman spectra and then determining the amounts of Asp occluded within the crystals. A lattice mode peak (at $\approx 283 \text{ cm}^{-1}$) and the strongest ν_1 peak (at $\approx 1085 \text{ cm}^{-1}$) were selected for analysis.⁴⁸ The calcite/Asp crystals showed rapid changes in the peak shift with the amount Asp occluded up to 1 mol%, before reaching a plateau, where this effect was greater for the lattice mode peak (4 cm^{-1}) than the ν_1 vibration peak (1.5 cm^{-1}) (Figure S9). The peak broadening showed a similar behavior, although the lattice mode peak continued to show

a gradual increase in width at higher occlusion levels. The changes in the lattice mode are indicative of disordering/ displacement of the carbonate groups, while changes in bond lengths will give rise to shifts in the vibration peaks.

Raman was employed in the current study to investigate the influence of occluded amino acids on the calcite structure, where the full width at half maximum (FWHM) of the carbonate peak at $\approx 1085 \text{ cm}^{-1}$ (C-O symmetrical stretching) was used as the metric for disorder. Crystals were precipitated in the same way as for SEM analysis, and Raman spectra were obtained using a Renishaw inVia system with optical microscope sample viewer and external stage control and operating with a wavelength of 785 nm. The sealing mats supporting the precipitated crystals were cut into sections with 6x8 studs, as per SEM, and these were then mounted onto glass microscope slides using double-sided carbon sticky tabs. Raman spectra were obtained from single crystals (rather than polycrystals) in the range 1050 to 1150 cm^{-1} with a scan time of 30 s (1 cm^{-1} resolution), and data was obtained from 3 different crystals in each sample.

The Raman data obtained clearly demonstrate that precipitation of calcite crystals in the presence of amino acids causes a broadening of the peaks, where this is necessarily associated with their occlusion in the lattice (Figure 6a). General trends of increasing FWHM with increasing $[\text{Ca}^{2+}]$ and $[\text{amino acid}]/[\text{Ca}^{2+}]$ are seen across Asp, Gly and Asn, but are most marked with Asp (Figure 6b). This is consistent with occlusion being promoted both at higher [Asp] and higher supersaturations, where the latter correlates with an increase in the density of step edges and kink sites,⁴⁹ which translates into higher occlusion levels. This effect was much less pronounced with Glu and Asn, and no such trend was observed for Val.

Calcium Carbonate Yield and Quantification of Amino Acid Incorporation: While the effects of additives on crystal morphologies have been well-studied, much less is known about the incorporation of small organic molecules within single crystals, and how this is governed by the solution conditions. The quantities of Asp, Glu, Asn and Val occluded within calcite single crystals was determined as a function of the initial $[\text{Ca}^{2+}]$ and $[\text{amino acid}]/[\text{Ca}^{2+}]$ by dissolving the amino acid/calcite crystals using EDTA, and then quantifying the amounts of liberated amino acids using a derivitization reaction and fluorimetric assay (Figure S8a). The concentration of amino acid in solution can then be determined using a calibration curve (Figure S8b).⁵⁰ In order to determine the occlusion efficiency it was also necessary to quantify the amount of CaCO_3 present in each well. This was achieved by dissolving the crystals in acetate buffer and then determining the $[\text{Ca}^{2+}]$ using a calcein chelation-based fluorimetric assay.⁵¹ Calcein fluorescence in basic solutions is quenched, but is recovered upon chelation to Ca^{2+} ions (Figure S9a). $[\text{Ca}^{2+}]$ was determined

from the fluorescence emission signal and compared with calibration curves prepared with known $[\text{Ca}^{2+}]$. This approach was adopted as traditional gravimetric methods are incompatible with our high-throughput approach.

Full experimental details are provided in the Supporting Information. Briefly, the crystallization reactions were conducted in Millipore Solvintert 0.45 μm hydrophilic filter plates, where these enable bleaching, washing, rinsing and drying of the crystals to be carried out by sequential removal of liquid from each well by filtration on a vacuum manifold. This procedure ensures that trace amounts of amino acids remaining on the surfaces of the crystals or the well plates are removed, while ensuring that there is minimal loss of crystal products. All aqueous stock solutions were transferred to the filter plate using a liquid handling pipetting workstation. Calibration curves of known [amino acid] or $[\text{Ca}^{2+}]$ were also prepared using the liquid handling pipetting workstation using the appropriate buffer, and the fluorescent reporting solutions (for amino acids or $[\text{Ca}^{2+}]$) were added to the experimental and calibration columns immediately prior to fluorescence analysis. The $[\text{Ca}^{2+}]$ determined from the solubilized crystals was always lower than the theoretical maximum calculated on the basis of the solubility product of calcite (Figure S9b), where this can be attributed to the effect of the amino acids on the solution supersaturation, and some inevitable loss of product during bleaching and washing. These values were then used to quantify the amounts of amino acid incorporated. The occlusion of Asp, Glu and Asn increased with the initial $[\text{Ca}^{2+}]$ and the [amino acid]/ $[\text{Ca}^{2+}]$ ratio (Figure 7). Asp was incorporated to the highest degree, reaching a maximum value of 3.03 mol% under conditions $[\text{Ca}^{2+}] = [\text{CO}_3^{2-}] = 10 \text{ mM}$ and $[\text{Asp}]/[\text{Ca}^{2+}] = 1.5$. In analogous experiments, Glu and Asn were incorporated at 0.92 and 0.55 mol% respectively. Non-linear incorporation trends were observed between the amount of amino acid incorporated and [amino acid]/ $[\text{Ca}^{2+}]$ at a fixed $[\text{Ca}^{2+}]$, where the efficiency of incorporation decreases as [amino acid]/ $[\text{Ca}^{2+}]$ increases. The quantities of Val incorporated were very low, reaching a maximum of 0.09 mol%, and no trends were recorded with respect to occlusion and the solution conditions. That the amino acids with acidic side-chains occlude most efficiently is in good agreement with previous studies, and the data provides further confirmation that Asp incorporates significantly more readily than Glu.¹⁴

DISCUSSION

The methodology developed here enables large arrays of experiments to be prepared simultaneously, using identical stock solutions and an accurate liquid handling workstation. All of the experiments are then conducted at the same temperature, and run for identical times. Finally, the crystalline products from each experiment are simultaneously prepared for analysis using common stock reagents, and the analyses performed using automated/ semi-automated procedures. As such, our high throughput method is ideally suited to the exploration of a broad reaction space, and for the reliable investigation of property trends using a suite of characterization methods. The inter-relationships between different properties, including morphology, the rate of precipitation, lattice disorder and additive incorporation can therefore be readily identified.

While the effects of amino acids on calcium carbonate precipitation have of course been addressed in the literature, studies have typically focused on their influence over a small number of crystal properties, such as polymorph or morphology.^{40, 46, 52, 53} Our approach facilitates a more holistic approach and clearly shows, for example, that the ability of additives to stabilize the initial ACC phase correlates with a stronger effect on morphology, lattice disorder and additive occlusion within the crystal lattice. With the demonstration that Asp has the greatest effect on CaCO₃ precipitation and crystal properties, followed by Glu and Asn, and that Val has negligible effect, our data are in excellent agreement with the literature,^{14, 54} confirming the reliability of our approach.

A particular innovation of our study is the development of a high throughput strategy, based upon fluorescence spectroscopy, for readily quantifying the amounts of the amino acids occluded within the CaCO₃ crystals. Indeed, while the effects of organic additives on CaCO₃ precipitation have been well-studied, comparatively little is known about their occlusion within the crystal lattice, and whether signatures of occlusion are seen in other physical properties. Gravimetric-based analyses have previously been used to quantify the biomacromolecules occluded within CaCO₃ biominerals, where the macromolecules are isolated after dissolution of the biomineral within a dialysis bag.⁵⁵ However, this method can only be used to quantify larger molecules. Alternatively, high performance liquid chromatography (HPLC) of dissolved crystals, followed by analysis of the fluorescence of derivatized amino acids, has been used to quantify the amounts of amino acids^{13, 14} and proteins^{56, 57} within CaCO₃ crystals and biominerals. Our strategy uses the same derivitization protocol to analyze the amino acids liberated from the CaCO₃ crystals, but prepares and analyses samples rapidly and in parallel, within the individual wells. Chromatography is only required if separation of different amino acids is

necessary. The excellent agreement of amino acid contents of crystals as determined by the traditional HPLC method and our high throughput strategy (Figure S10) confirms the validity of our approach.

Considering then the amino acid occlusion data in more detail, the solution conditions employed in our experiments yielded maximum occlusion levels of 3.4, 0.93, 0.55 and 0.09 mol% for Asp, Glu, Asn and Val respectively. This overall trend is comparable to that reported by Borukhin et al, who reported values of 0.8, 0.4, 0.1 and ≈ 0 mol% for Asp, Glu, Asn and Val,¹⁴ while Kim et al reported the occlusion of 3.9 mol% Asp within calcite single crystals.¹³ It is interesting then to correlate these occlusion data with the precipitation kinetics, structural information from Raman spectroscopy and the observed changes in crystal morphologies, where plots of the cross-correlations are shown in Figure 8. Asp had the strongest effect on all features, offering significant stabilization of ACC (through inhibition of the growth of calcite) (Figure 8i), a strong signature of occlusion in the Raman spectra (Figure 8ii and Figure S11 for clarity) and modifying morphologies at the lowest [amino acid]/[Ca²⁺] ratio (Figure 8iii). Comparing then with Glu, however, it is noted that although Glu also provides strong stabilization of ACC, and is active in changing the crystal morphologies, it occludes much less efficiently than Asp. Indeed, the cross-correlation data show that changes in crystal morphology are not strongly correlated with the property of additive occlusion (Figure 8iii), which demonstrates that significant levels of occlusion can occur without a change in crystal morphology.

The contrasting effects of the amino acids are intriguing. Their effects on ACC precipitation/crystallization and the crystal morphologies are consistent with the charge of the side group, where the negatively charged (under the experimental conditions) side groups of Asp and Glu are considered to interact with the Ca²⁺ ions at the crystal surface.⁴⁵ All of the amino acids studied are negatively charged under the experimental conditions, where the pI values for Asp, Glu, Asn and Val are 2.9, 3.2, 5.4 and 6 respectively. Modeling of the interaction of Asp molecules with calcite surfaces has also shown that these molecules preferentially bind to the symmetry-related acute step edges via specific stereochemistry.⁴⁶ With its carboxamide side chain, Asn binds significantly less strongly, while the hydrophobic side chain of Val results in minimal interaction with the growing calcite crystals. The process of occlusion is clearly more complex, however, and is strongly dependent on both the structure of the additive and its charge. Modelling studies have shown that Asp²⁻ molecules are occluded within the calcite lattice with a very good fit such that the carboxylic acid groups on Asp²⁻ replace the CO₃²⁻ groups on adjacent carbonate planes.¹³ With an extra methylene group in the side chain, Glu is expected to cause significantly more lattice strain.

It is also instructive to look at published data for the occlusion of glycine (Gly) within calcite, where this has been reported to reach levels of up to 7 mol%.¹³ Without an anionic side-group, Gly neither

binds as strongly to calcite as Asp nor fits as well within the lattice,¹³ but its high occlusion levels demonstrate that binding through the α -amino acid moieties is sufficient to drive incorporation. On exchange of the small H side-group of glycine for the larger carboxamide in Asn or isopropyl in Val, it can be expected that the binding strength will decrease and the lattice strain caused on occlusion would increase. That our data reveals a weak correlation in the ability of an amino acid to cause changes in crystal morphologies and to become occluded suggests that the “fit” of the amino acid within the crystal lattice is a significant determinant for whether occlusion will occur. While a full understanding of this process would necessarily require detailed modelling studies to understand every step of the incorporation process, experimental multi-variant studies screening a wide range of reaction parameters provide an invaluable means to identifying key reaction trends and building a full and un-biased picture of additive-directed crystallization over a wide range of conditions.

CONCLUSIONS

The methodology presented here offers a high-throughput approach for rapidly and systematically quantifying the effects of additives on crystal growth. Through the combination of a number of high-throughput and rapid-screening technologies, our methodology enables the streamlined preparation of crystalline materials and the characterization of the kinetics of their precipitation, together with the morphology, size, structure and compositions of the crystals. As further benefits of the approach, the simultaneous production of an array of reaction solutions provides control over the physical and chemical conditions, while automation vastly reduces sample preparation time and reduces experimental error. This strategy is therefore ideally suited to the comparison of a large number of samples, and the investigation of a wide reaction space. Indeed, the large number of potential variables in additive-directed crystallization experiments typically precludes the identification of reaction conditions which deliver the target product.³² While the current study focused on the control of calcium carbonate growth and properties using amino acids additives, our experimental design is undoubtedly quite general and could be readily adapted to a range of crystalline materials. Indeed, well plates are available that are resistant to many organic solvents, high acid/basic conditions, and temperatures of at least 200 °C. Other equipment used, including the well plate heater and shaker can provide careful temperature control and shaking for extended reaction times. It should therefore be possible to extend our methods to the synthesis of materials including functional oxides, semiconductor/metallic nanoparticles and even metal-organic frameworks. Further, with the ability to rapidly screen the structure/ property relationships of crystals generated under a wide range of reaction conditions, our methodology promises to identify reaction conditions that lead to materials

with optimized properties, while also generating new understanding of the mechanisms underlying additive-directed crystallization.

ASSOCIATED CONTENT

Supporting Information. Full experimental details, protocol overview schematics, experimental design maps; SEM, image analysis. Raman microscopy, calcium and amino acid quantification data; experimental set-up diagrams (Figures S1-S18). This material is available free of charge via the Internet at <http://pubs.acs.org>.

DATA AVAILABILITY

All data that support the findings of this study are available in the Research Data Leeds Repository with the identifier <http://doi.org/10.5518/69>.⁴²

AUTHOR INFORMATION

Corresponding Author

*email: F.Meldrum@leeds.ac.uk

†Current address: Paul Scherrer Institute, 5232 Villingen PSI, Switzerland

Notes

The authors declare no competing financial interest.

ACKNOWLEDGMENT

This work was supported by an Engineering and Physical Sciences Research Council (EPSRC) Leadership Fellowship (FCM and JI, EP/H005374/1) and an EPSRC Programme Grant (grant EP/I001514/1) which funds the Materials Interface with Biology (MIB) consortium (FCM and DCG).

REFERENCES

- (1) Song, R. Q.; Colfen, H., *Crystengcomm* **2011**, *13*, 1249-1276.
- (2) Meldrum, F. C.; Colfen, H., *Chem. Revs.* **2008**, *108*, 4332-4432.
- (3) Shtukenberg, A. G.; Lee, S. S.; Kahr, B.; Ward, M. D., Manipulating Crystallization with Molecular Additives. In *Ann. Rev. Chem. Biomol. Eng.*, Prausnitz, J. M.; Doherty, M. F.; Segalman, R. A., Eds. Annual Reviews: Palo Alto, 2014; Vol. 5, pp 77-96.
- (4) Lowenstam, H. A.; Weiner, S., *On Biomineralization*. ed.; Oxford University Press: New York, 1989.
- (5) Mann, S., *Biomineralization: Principles and Concepts in Bioinorganic Materials Chemistry*. ed.; Oxford University Press: Oxford, U.K., 2001; pp 240.
- (6) Weiner, S.; Addadi, L., Crystallization Pathways in Biomineralization. In *Ann. Rev. Mater. Res.*, Clarke, D. R.; Fratzl, P., Eds. Annual Reviews: Palo Alto, 2011; Vol. 41, pp 21-40.
- (7) Weiner, S.; Addadi, L.; Wagner, H. D., *Mater. Sci. Eng. C* **2000**, *11*, 1-8.
- (8) Berman, A.; Hanson, J.; Leiserowitz, L.; Koetzle, T.; Weiner, S.; Addadi, L., *J. Phys. Chem.* **1993**, *97*, 5162-70.
- (9) Pokroy, B.; Fitch, A. N.; Marin, F.; Kapon, M.; Adir, N.; Zolotoyabko, E., *J. Struc. Biol.* **2006**, *155*, 96-103.
- (10) Phillips, B. L.; Lee, Y. J.; Reeder, R. J., *Environ. Sci. Technol.* **2005**, *39*, 4533-4539.
- (11) Metzler, R. A.; Tribello, G. A.; Parrinello, M.; Gilbert, P., *J. Am. Chem. Soc.* **2010**, *132*, 11585-11591.
- (12) Schenk, A. S.; Zlotnikov, I.; Pokroy, B.; Gierlinger, N.; Masic, A.; Zaslansky, P.; Fitch, A. N.; Paris, O.; Metzger, T. H.; Colfen, H.; Fratzl, P.; Aichmayer, B., *Adv. Func. Mater.* **2012**, *22*, 4668-4676.
- (13) Kim, Y. Y.; Carloni, J. D.; Demarchi, B.; Sparks, D.; Reid, D. G.; Kunitake, M. E.; Tang, C. C.; Duer, M. J.; Freeman, C. L.; Pokroy, B.; Penkman, K.; Harding, J. H.; Estroff, L. A.; Baker, S. P.; Meldrum, F. C., *Nature Mater.* **2016**, <http://dx.doi.org/10.1038/nmat4631>.
- (14) Borukhin, S.; Bloch, L.; Radlauer, T.; Hill, A. H.; Fitch, A. N.; Pokroy, B., *Adv. Func. Mater.* **2012**, *22*, 4216-4224.
- (15) VeintemillasVerdaguer, S., *Prog. Cryst. Growth Charac. Mater.* **1996**, *32*, 75-109.
- (16) Sangwal, K.; Benz, K. W., *Prog. Cryst. Growth Charac. Mater.* **1996**, *32*, 135-169.
- (17) Morantz, D. J.; Mathur, K., *Nature* **1970**, *226*, 638-&.
- (18) Kim, Y. Y.; Ganesan, K.; Yang, P. C.; Kulak, A. N.; Borukhin, S.; Pechook, S.; Ribeiro, L.; Kroger, R.; Eichhorn, S. J.; Armes, S. P.; Pokroy, B.; Meldrum, F. C., *Nature Mater.* **2011**, *10*, 890-896.
- (19) Brif, A.; Ankonina, G.; Drathen, C.; Pokroy, B., *Adv. Mater.* **2014**, *26*, 477-481.
- (20) Kahr, B.; Gurney, R. W., *Chem. Revs.* **2001**, *101*, 893-951.

- (21) Kulak, A. N.; Semsarilar, M.; Kim, Y. Y.; Ihli, J.; Fielding, L. A.; Cespedes, O.; Armes, S. P.; Meldrum, F. C., *Chem. Sci.* **2014**, *5*, 738-743.
- (22) Kulak, A. N.; Yang, P. C.; Kim, Y. Y.; Armes, S. P.; Meldrum, F. C., *Chem. Commun.* **2014**, *50*, 67-69.
- (23) Adam, M.; Wang, Z. Y.; Dubavik, A.; Stachowski, G. M.; Meerbach, C.; Soran-Erdem, Z.; Rengers, C.; Demir, H. V.; Gaponik, N.; Eychmuller, A., *Adv. Func. Mater.* **2015**, *25*, 2638-2645.
- (24) Lose, E.; Wilson, R. M.; Seshadri, R.; Meldrum, F. C., *J. Cryst. Growth* **2003**, *254*, 206-218.
- (25) Elzinga, E. J.; Reeder, R. J., *Geochim. Cosmochim. Acta* **2002**, *66*, 3943-3954.
- (26) Tang, Y. Z.; Elzinga, E. J.; Lee, Y. J.; Reeder, R. J., *Geochim. Cosmochim. Acta* **2007**, *71*, 1480-1493.
- (27) Kralj, D.; Kontrec, J.; Brecevic, L.; Falini, G.; Nothig-Laslo, V., *Chem. Eur. J.* **2004**, *10*, 1647-1656.
- (28) Elali, A.; Barbin, V.; Calas, G.; Cervelle, B.; Ramseyer, K.; Bouroulec, J., *Chem. Geol.* **1993**, *104*, 189-202.
- (29) Cho, K. R.; Kim, Y. Y.; Yang, P. C.; Cai, W.; Pan, H. H.; Kulak, A. N.; Lau, J. L.; Kulshreshtha, P.; Armes, S. P.; Meldrum, F. C.; De Yoreo, J. J., *Nature Commun.* **2016**, *7*, 10187
- (30) Kim, Y. Y.; Ribeiro, L.; Maillot, F.; Ward, O.; Eichhorn, S. J.; Meldrum, F. C., *Adv. Mater.* **2010**, *22*, 2082-2086.
- (31) Munoz-Espi, R.; Qi, Y.; Lieberwirth, I.; Gomez, C. M.; Wegner, G., *Chem. Eur. J.* **2006**, *12*, 118-129.
- (32) Bawazer, L. A.; Ihli, J.; Comyn, T. P.; Critchley, K.; Empson, C. J.; Meldrum, F. C., *Adv. Mater.* **2015**, *27*, 223-227.
- (33) Morissette, S. L.; Almarsson, O.; Peterson, M. L.; Remenar, J. F.; Read, M. J.; Lemmo, A. V.; Ellis, S.; Cima, M. J.; Gardner, C. R., *Adv. Drug Delivery Revs.* **2004**, *56*, 275-300.
- (34) Luft, J. R.; Snell, E. H.; DeTitta, G. T., *Expert Op. Drug Disc.* **2011**, *6*, 465-480.
- (35) Hui, R.; Edwards, A., *J. Struc. Biol.* **2003**, *142*, 154-161.
- (36) Koinuma, H.; Takeuchi, I., *Nature Mater.* **2004**, *3*, 429-438.
- (37) Potyrailo, R.; Rajan, K.; Stoewe, K.; Takeuchi, I.; Chisholm, B.; Lam, H., *ACS Comb. Sci.* **2011**, *13*, 579-633.
- (38) Kafizas, A.; Parkin, I. P., *Chem. Soc. Revs.* **2012**, *41*, 738-781.
- (39) Woodhouse, M.; Parkinson, B. A., *Chem. Soc. Revs.* **2009**, *38*, 197-210.
- (40) Wang, Y. W.; Kim, Y. Y.; Stephens, C. J.; Meldrum, F. C.; Christenson, H. K., *Cryst. Growth Des.* **2012**, *12*, 1212-1217.
- (41) Ihli, J.; Kim, Y. Y.; Noel, E. H.; Meldrum, F. C., *Adv. Func. Mater.* **2013**, *23*, 1575-1585.

- (42) Green, D. C.; Ihli, J.; Kim, Y.-Y.; Chong, S. Y.; Lee, P. A.; Empson, C. J.; Meldrum, F. C., *Research Data Leeds Repository* **2016**, <http://doi.org/10.5518/69>.
- (43) De Yoreo, J. J.; Vekilov, P. G., Principles of crystal nucleation and growth. In *Biom mineralization*, Dove, P. M.; DeYoreo, J. J.; Weiner, S., Eds. Mineralogical Soc America: Washington, 2003; Vol. 54, pp 57-93.
- (44) Paquette, J.; Reeder, R. J., *Geochim. Cosmochim. Acta* **1995**, *59*, 735-749.
- (45) Elhadj, S.; De Yoreo, J. J.; Hoyer, J. R.; Dove, P. M., *Proc. Nat. Acad. Sci. USA* **2006**, *103*, 19237-19242.
- (46) Orme, C. A.; Noy, A.; Wierzbicki, A.; McBride, M. T.; Grantham, M.; Teng, H. H.; Dove, P. M.; DeYoreo, J. J., *Nature* **2001**, *411*, 775-779.
- (47) Noel, E. H.; Kim, Y. Y.; Charnock, J. M.; Meldrum, F. C., *Crystengcomm* **2013**, *15*, 697-705.
- (48) Kontoyannis, C. G.; Vagenas, N. V., *Analyst* **2000**, *125*, 251-255.
- (49) De Yoreo, J. J.; Zepeda-Ruiz, L. A.; Friddle, R. W.; Qiu, S. R.; Wasylenki, L. E.; Chernov, A. A.; Gilmer, G. H.; Dove, P. M., *Cryst. Growth Des.* **2009**, *9*, 5135-5144.
- (50) Mueller, C.; Fonseca, J. R.; Rock, T. M.; Krauss-Etschmann, S.; Schmitt-Kopplin, P., *J Chromatogr A* **2014**, *1324*, 109-114.
- (51) Pokrzywnicka, M.; Fiedoruk, M.; Koncki, R., *Talanta* **2012**, *93*, 106-110.
- (52) Chuajiw, W.; Takatori, K.; Igarashi, T.; Hara, H.; Fukushima, Y., *J. Cryst. Growth* **2014**, *386*, 119-127.
- (53) Xie, A. J.; Shen, Y. H.; Zhang, C. Y.; Yuan, Z. W.; Zhu, X. M.; Yang, Y. M., *J. Cryst. Growth* **2005**, *285*, 436-443.
- (54) Picker, A.; Kellermeier, M.; Seto, J.; Gebauer, D.; Colfen, H., *Zeit. Kristal.* **2012**, *227*, 744-757.
- (55) Gotliv, B. A.; Addadi, L.; Weiner, S., *Chembiochem* **2003**, *4*, 522-529.
- (56) Demarchi, B.; Rogers, K.; Fa, D. A.; Finlayson, C. J.; Milner, N.; Penkman, K. E. H., *Quat. Geochron.* **2013**, *16*, 144-157.
- (57) Penkman, K. E. H.; Kaufman, D. S.; Maddy, D.; Collins, M. J., *Quat. Geochron.* **2008**, *3*, 2-25.

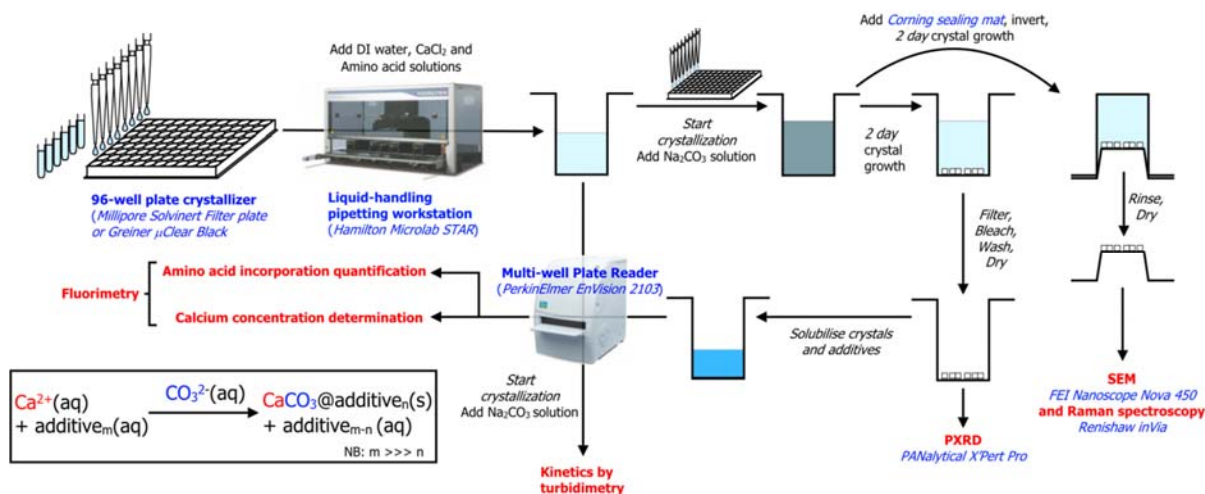


Figure 1: Overview of high-throughput methodology. Schematic diagram showing the high throughput experimental process and equipment employed to precipitate calcite in the presence of amino acids, quantify amino acid incorporation in amino acid/calcite crystals, undertake kinetic analysis based on turbidimetric measurements, and perform morphological and structural characterisation of the crystals. A general equation for the reaction is also given, where the additives are Asp, Glu, Asn or Val.

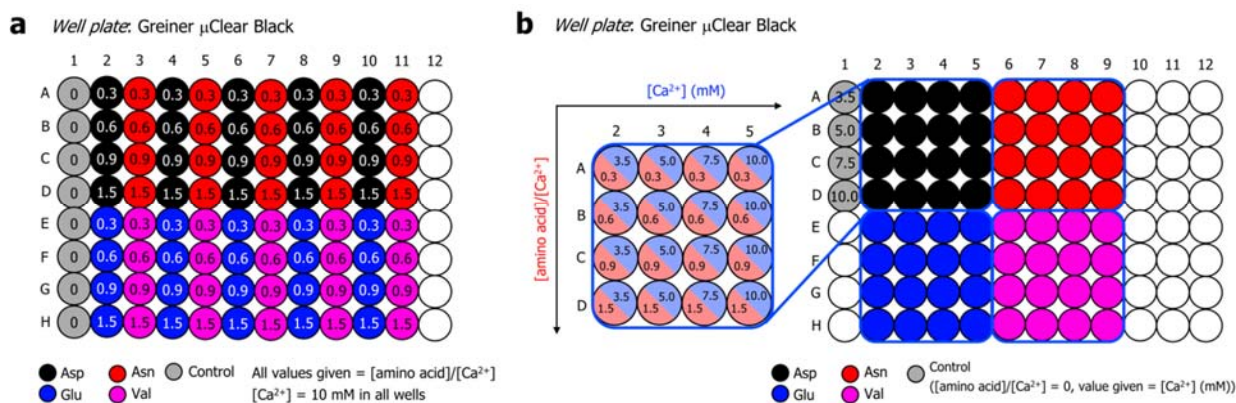


Figure 2: Experimental design. Well plate 'map' showing the experimental design of the plates used for kinetics (a) and Raman, SEM and pXRD (b) studies. The different colours correspond to the different amino acids in solution (Asp = black, Glu = blue, Asn = red, Val = pink and no amino acid (control) = grey). In (b), each 4 x 4 array per amino acid contains the same [Ca²⁺] and [amino acid]/ [Ca²⁺] values as shown in the detailed diagram on the left, where the numbers with a red background correspond to [amino acid]/ [Ca²⁺] number with a blue background correspond to [Ca²⁺].

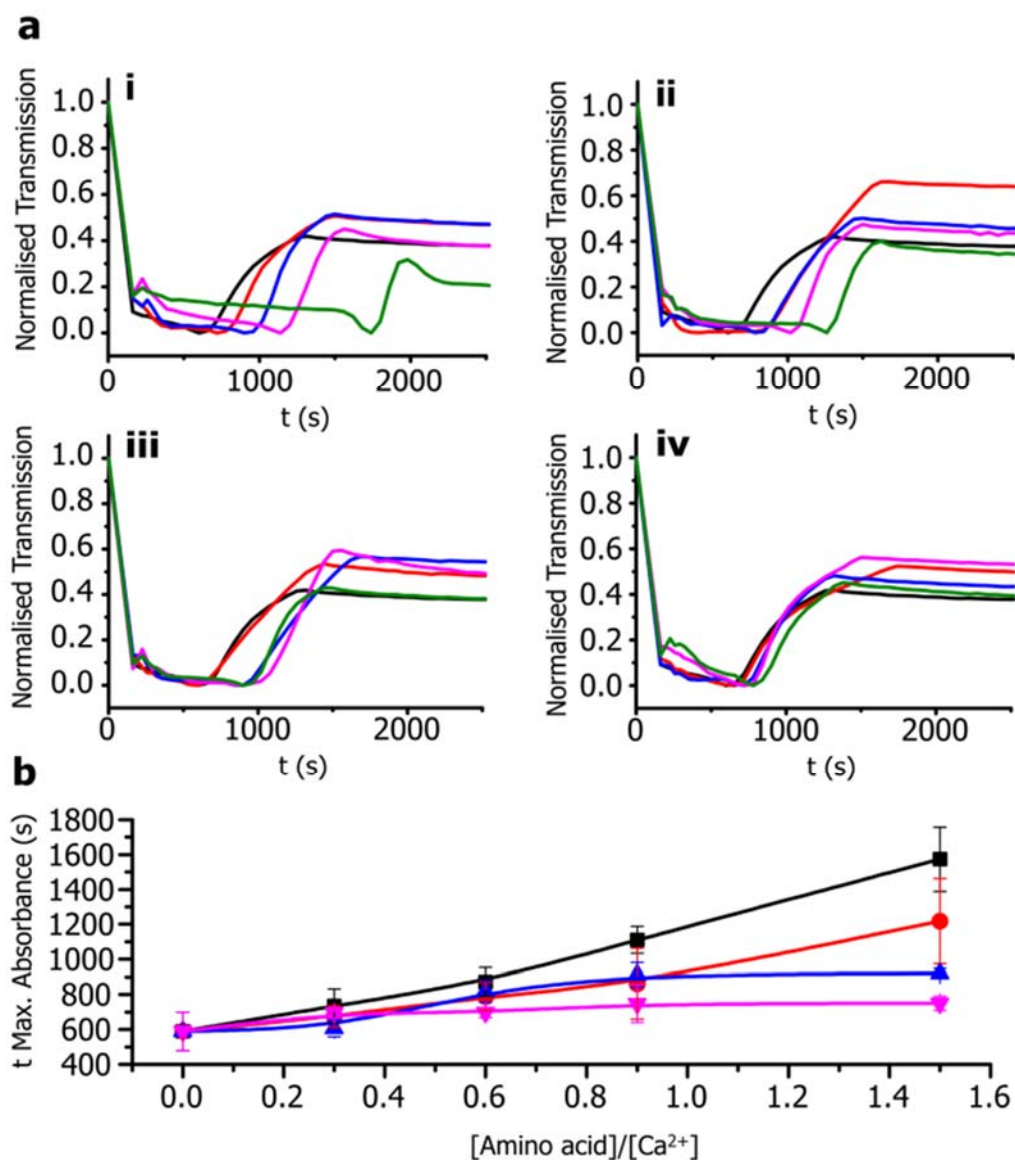


Figure 3: Turbidimetric analysis of precipitation kinetics. (a) Typical time vs normalized transmitted light plots during the precipitation of calcium carbonate in the presence of (i) Asp, (ii) Glu, (iii) Asn and (iv) Val. In all cases the plots are shown for each $[\text{amino acid}]/[\text{Ca}^{2+}] = 0$ (black), 0.3 (red), 0.6 (blue), 0.9 (pink) and 1.5 (green), where the reaction solutions comprise $[\text{CO}_3^{2-}] = [\text{Ca}^{2+}] = 10 \text{ mM}$. (b) Time of maximum absorbance vs $[\text{amino acid}]/[\text{Ca}^{2+}]$ plots show the greater influence of Asp (black) on precipitation as compared to Glu (red), Asn (blue) and Val (pink).

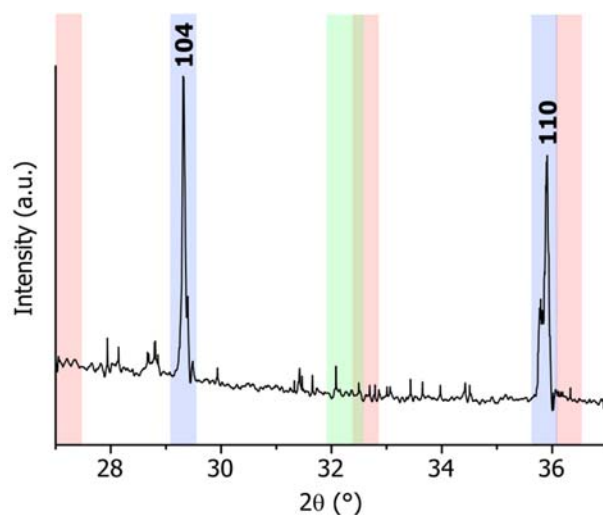


Figure 4: Polymorph identification with pXRD. A typical diffractogram, after background removal, obtained using an automated, high-throughput protocol for polymorph identification. The peaks detected corresponded to calcite only (peak regions denoted in blue), and no aragonite (red) or vaterite (green) was identified in any of the wells.

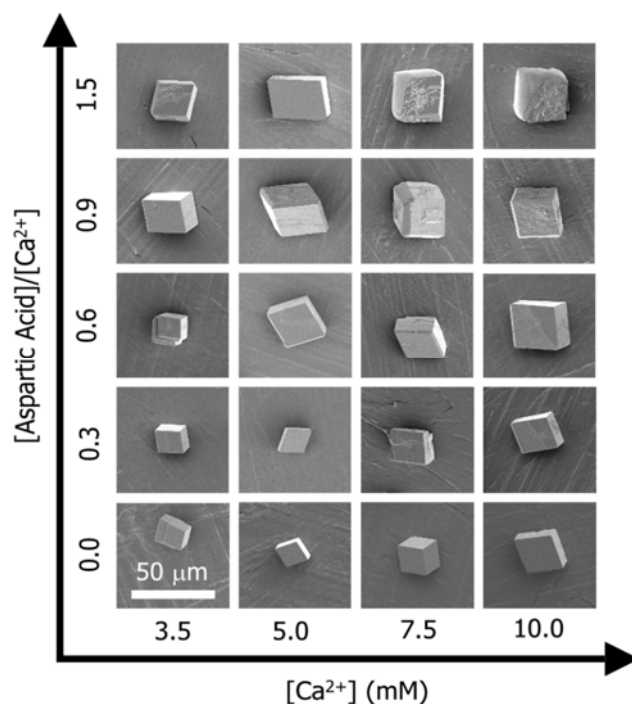


Figure 5: Shape analysis by SEM. Micrographs of calcite single crystals observed using high-throughput sample preparation methods grown in the presence of Asp. Micrographs are arranged with increasing [Ca²⁺] and [amino acid]/[Ca²⁺], such that the effect of both parameters on the shape can be easily seen.

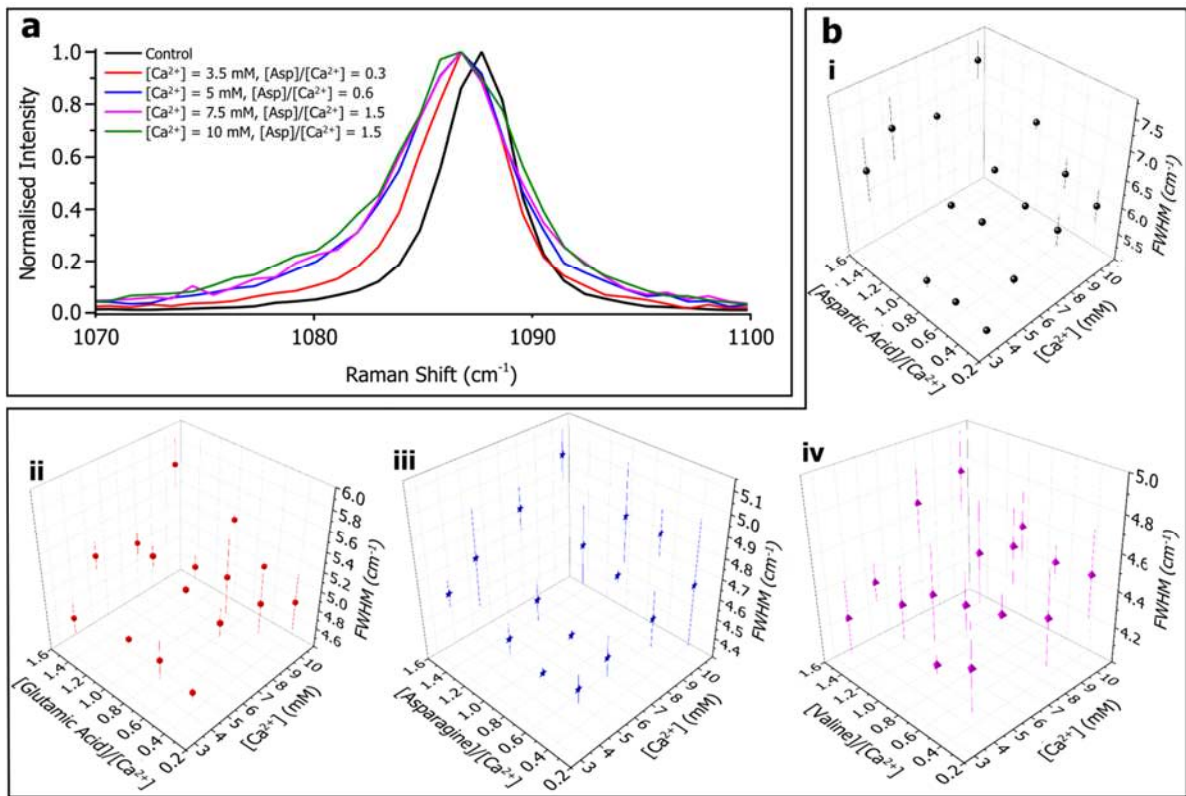


Figure 6: Structural analysis by Raman microscopy. a) Selected Raman spectra taken from calcite single crystals grown under various conditions in the presence of Asp. Specific conditions are given in the legend. The broadening can be seen as an effect of changing conditions, or of increasing Asp incorporation, where spectra correspond to samples containing 0 (black), 0.35 (red), 1.04 (blue), 2.38 (pink) and 3.04 (green) mol% Asp. b) 3D (XYZ) plots describing the change in the breadth of the peak at 1085 cm⁻¹ (C-O symmetrical stretching) in Raman spectra taken from calcite single crystals grown in the presence of (i) Asp, (ii) Glu, (iii) Asn and (iv) Val.

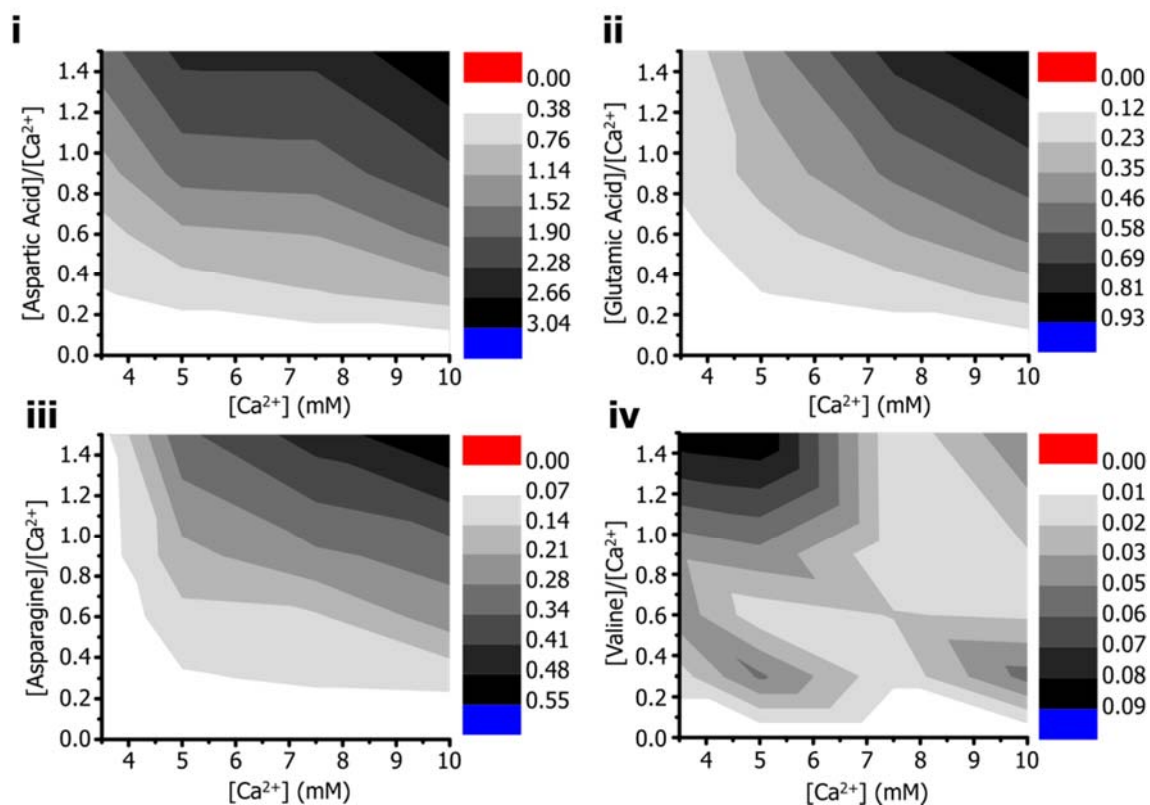


Figure 7: High-throughput quantification of amino acid incorporation. Contour plots (XYZ; X = $[Ca^{2+}]$, Y = $[amino\ acid]/[Ca^{2+}]$ and Z = incorporated amino acid (mol%), white to black = lowest to highest) of quantified incorporated (i) Asp, (ii) Glu, (iii) Asn and (iv) Val in calcite/amino acid crystals.

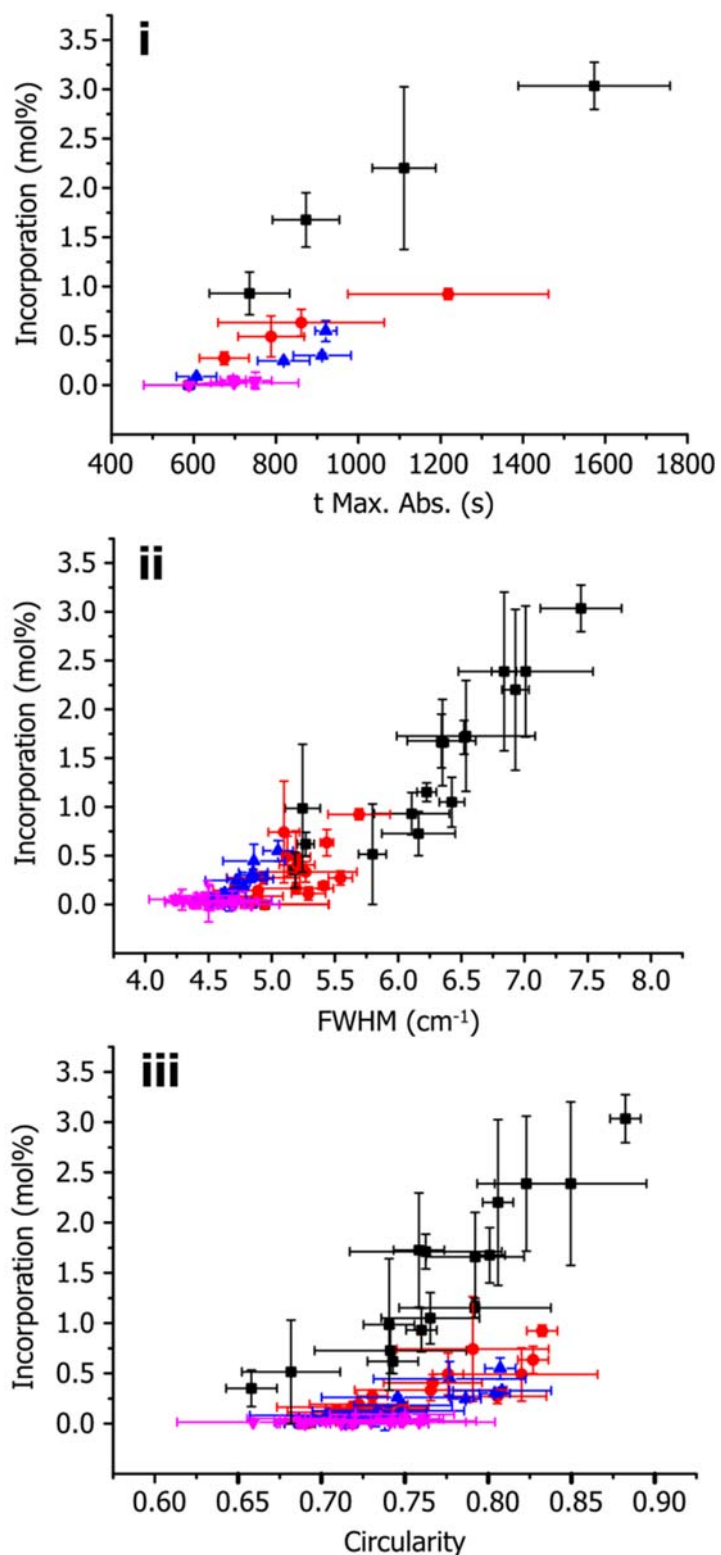


Figure 8: Cross-referencing data sets for observation of trends. Values from amino acid quantification studies were plotted against (i) kinetic, (ii) Raman and (iii) shape analysis data. Amino acids are denoted as such: Asp (black circle), Glu (red square), Asn (blue triangle) and Val (pink inverted triangle).